PNAS RESEARCH ARTICLE | SUSTAINABILITY SCIENCE

Infrastructure form shapes equitable access to essential services under flooding in Philippine cities

Noam Anglo[a], Eileen Chen[b], Sophie Pesek[c,1], Kevin Skinner[d], and Anders Vestrum[e]

This manuscript was compiled on May 8, 2026

Urban flooding is becoming an increasingly pressing issue due to climate change. Flood risk in cities is usually assessed by overlaying inundation maps with exposed population and assets. That view misses an important mechanism of harm: residents can lose access to essential services when flooded road segments sever routes, even if neither the resident nor the facility is directly flooded. Evaluating ten cities in the Philippines, one of the most flood-affected countries in the world, we develop a reproducible network-accessibility framework that combines OpenStreetMap road networks and service locations, LandScan population grids, Project NOAH flood hazard layers, and 2020 Philippine census demographics. We validate flood hazard using independent multi-source observations, including AI4G Sentinel-1 detections, PhilSA satellite flood extents, and Groundsource event data. We find further evidence of mobility disruptions by validating Reddit threads of infrastructure outages during flood events. Baseline results show substantial variation in road-network hierarchy, facility coverage, and pre-flood access to hospitals, schools, markets, and pharmacies. Betweenness centrality is highly concentrated in every city, with Gini coefficients between 0.82 and 0.93, indicating that a small set of links can structure a large share of shortest-path flow. The flood-disruption model removes road edges intersecting medium- or high-depth Project NOAH polygons and recomputes enhanced two-step floating catchment area accessibility to identify direct and indirect access losses. Independent satellite observations provide strong support for NOAH hazard patterns, while Groundsource offers auxiliary evidence but lower spatial precision, especially in dense urban areas such as Manila. We then aggregate modeled disruption to barangays and compare demographic profiles across city-specific disruption quintiles to describe which populations are most exposed to indirect service-access losses.

flood resilience | road networks | accessibility | infrastructure equity | Philippines

Significance

Flood studies often map where water goes, but communities also lose access when flooded roads sever routes to hospitals, schools, markets, and pharmacies. This study links flood hazard maps, road networks, population grids, and essential-service locations to measure the indirect loss of access across Philippine cities, then compares these disruptions to barangay-level demographic profiles to evaluate which populations are most impacted. The framework helps identify neighborhoods that may be isolated outside inundation zones and road segments whose protection would preserve the greatest service access. It offers a reproducible way to translate flood exposure into equitable infrastructure priorities for local planners working under scarce adaptation budgets.

Flooding is a central infrastructure and equity challenge for Philippine cities. The Philippines ranked first in the 2025 WorldRiskIndex, and the report's local flood-exposure analysis identifies several Philippine provinces as among the highest-risk subnational areas (1). PAGASA reports that the Philippine Area of Responsibility receives roughly 20 tropical cyclones per year, with about eight or nine crossing the country (2). Recent evidence also suggests that the frequency of super typhoons in the Philippine Area of Responsibility increased sharply after the late 1990s (3). These hazards operate through infrastructure systems: roads that fail during floods can fragment cities, delay emergency response, and isolate households from routine services.

Existing work provides pieces of this problem. Global and national flood-network studies show that local inundation can produce nonlocal road-network failure (4, 5). City-scale studies have overlaid flood footprints on road graphs to measure topological degradation (6), while accessibility studies use two-step floating catchment area methods to estimate spatial service availability under ordinary conditions (7, 8). However, many accessibility applications treat

Author affiliations: [a]Development Engineering, University of California, Berkeley, Berkeley, CA 94720; [b]Department of City and Regional Planning, University of California, Berkeley, Berkeley, CA 94720; [c]Energy and Resources Group, University of California, Berkeley, Berkeley, CA 94720; [d]School of Information, University of California, Berkeley, Berkeley, CA 94720; [e]Department of Electrical Engineering and Computer Sciences, University of California, Berkeley, Berkeley, CA 94720

N.A. led project framing and Philippine context; E.C. developed the network, routing, and accessibility methodology; S.P. originated the project scope, led demographic data analysis and figure development; K.S. developed the Reddit corpus and behavioral validation pipeline; A.V. led cross-source flood validation, network-criticality framing, and manuscript integration. All authors contributed to writing and interpretation.

The authors declare no competing interest.

[1]Correspondence should be addressed to S.P. spesek@berkeley.edu

networks as static, while many flood-network studies focus on connectivity rather than supply, demand, and competition for services.

We bridge these streams by coupling real flood-hazard footprints with network-routed enhanced two-step floating catchment area (E2SFCA) accessibility. The empirical setting is ten Philippine cities selected from provinces highlighted by the WorldRiskReport local flood-exposure analysis. For each city, we combine OpenStreetMap roads and facilities (9, 10), LandScan 2023 population grids (11), and Project NOAH flood hazard layers (12, 13). We validate flood hazard using multiple independent observational datasets, including satellite-derived flood detections and event-based reporting sources.

This analysis asks: **How does pre-flood road network topology in the Philippines shape access to essential services during flood scenarios, and how are these disruptions distributed across populations?** We answer this question by first characterizing baseline road-network structure and facility geography across ten Philippine cities, then estimating pre-flood access to hospitals, schools, markets, and pharmacies, and finally simulating flood-related road disruptions to identify direct and indirect losses in service access. To answer the population-distribution component of the question, we link modeled accessibility disruption to barangay-level census summaries, allowing the analysis to move from road and facility failures to the demographic profiles of communities exposed to those failures (14).

Related work. The methods used in this project are well established, but they have largely developed in separate strands. Street-network analysis tools such as OSMnx have made it possible to construct, route over, and compare urban road networks in a reproducible way using open data (15). Recent work on travel-time prediction from sparse open data further shows that credible edge-level speed estimates can be derived from OpenStreetMap and limited free training data, reducing reliance on proprietary traffic feeds (16). In parallel, spatial-accessibility methods such as the enhanced two-step floating catchment area method introduced distance-decay weights to reflect declining willingness or ability to travel with time or distance (17), while comparisons of 2SFCA variants show how catchment thresholds and decay functions shape measured accessibility (18). These tools provide the foundation for estimating access to hospitals, schools, markets, and pharmacies, but most accessibility applications treat road networks as static rather than vulnerable to disruption.

Flood-network research addresses the disruption side of the problem. Wang et al. show that local flooding can induce large-scale abrupt failures in road networks, with flood-induced failures behaving differently from random or targeted attacks (19). Fan et al. model flood propagation and recession across urban road networks as a contagion process, showing how road segments transition through susceptible, exposed, flooded, and recovered states over time (20). Boeing and Ha extend the disruption perspective globally by simulating street-network failures across urban areas, though their approach relies on synthetic removal scenarios rather than local flood footprints (21). At the city scale, Casali and Heinimann overlay flood maps onto the Zurich road

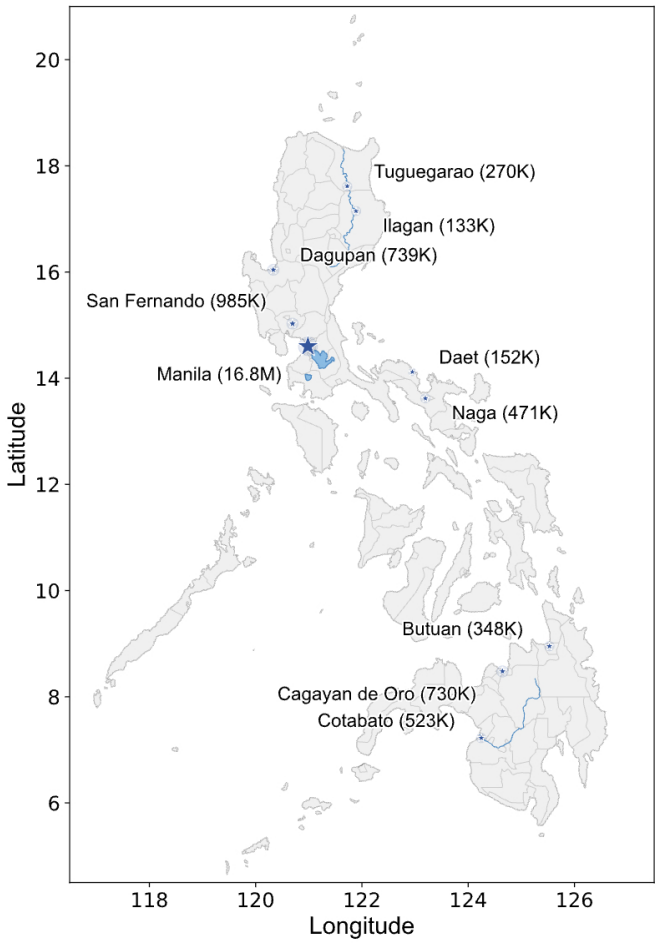

Fig. 1. Study cities in the Philippines, labeled by LandScan-estimated population inside each analysis radius. Cities were selected from provinces highlighted as high-exposure areas in the WorldRiskReport local flood-exposure analysis.

network to measure topological degradation (22), while Loreti et al. show that standard percolation metrics can miss realistic accessibility losses during spatially correlated floods (23). Gangwal and Dong move further toward service access by identifying early-warning thresholds at which accessibility to hospitals, emergency medical services, and shelters begins to decline rapidly during flood events (24).

A related literature highlights why disruption should be measured not only as network damage, but as unequal loss of access. Esmalian et al. use location-based mobility data during Hurricane Harvey to show that areas not classified as food deserts under normal conditions can become functionally inaccessible during disasters (25). Best et al. similarly show that isolation risk from sea-level rise can emerge before direct inundation, with disproportionate exposure among Black, Hispanic, renter, and older-adult populations in the United States (26). Kephart et al. document large socioeconomic disparities in neighborhood flood exposure across Latin American cities, reinforcing that flood risk is socially patterned rather than merely hydrological (27). Together, these studies suggest that flood vulnerability depends on the interaction among hazard exposure, road-network structure, facility geography, and the spatial distribution of population.

Table 1. Study-city scale and road-network structure.

City	Population	Nodes	Edges	Avg. deg.	Max BC	BC Gini	Hosp.
Manila	16,805,098	81,760	204,883	5.01	0.234	0.931	286
San Fernando	985,309	18,647	45,375	4.87	0.241	0.890	40
Dagupan	739,388	6,605	15,307	4.63	0.260	0.858	20
Cagayan de Oro	729,578	11,301	27,689	4.90	0.175	0.869	13
Cotabato	523,027	3,012	7,405	4.92	0.459	0.833	10
Naga	470,868	5,852	15,238	5.21	0.258	0.845	9
Butuan	347,820	5,823	14,564	5.00	0.297	0.841	12
Tuguegarao	269,517	3,944	9,693	4.92	0.371	0.845	11
Daet	152,260	2,472	6,595	5.34	0.378	0.820	7
Ilagan	133,307	2,762	6,976	5.05	0.485	0.837	2

Population is LandScan 2023 population within each study radius. Nodes and edges come from drivable OpenStreetMap graphs retrieved with OSMnx. BC denotes betweenness centrality. Hospital counts are OpenStreetMap points of interest before registry-based quality assurance.

This project bridges these literatures by coupling real flood-hazard footprints with network-routed E2SFCA accessibility. Unlike studies that focus only on topological degradation, the analysis estimates how flood-disrupted roads change modeled access to essential services after accounting for population demand, facility supply, and distance decay. Unlike mobility-data approaches, the framework relies on reproducible open or public data sources, making it transferable to settings where proprietary mobility traces are unavailable. This is especially important in the Philippine context, where Project NOAH provides locally relevant flood-hazard layers and where flood-disrupted mobility has direct empirical support: Mamuyac et al. show from Metro Manila CCTV footage that flood depths above roughly 25 cm cause lane closures and reduce vehicle flow by 40–70% per lane-kilometer as closures increase (28). The resulting framework treats flood vulnerability not simply as inundation exposure, but as the modeled loss of access that occurs when road failures sever routes between residents and essential services.

Study areas and network structure. The study sample spans a large urban hierarchy, from Metro Manila's 16.8 million LandScan-estimated residents to Ilagan's 133,000. The corresponding road networks contain 142,178 nodes and 353,725 directed edges across all cities, with Manila accounting for more than half of both nodes and edges (Table 1; Fig. 1). Average node degree is relatively stable, ranging from 4.63 in Dagupan to 5.34 in Daet, which suggests that local intersection connectivity alone is not a strong differentiator across the sample.

The more important structural variation is hierarchy. Betweenness centrality is concentrated in every city: the betweenness Gini ranges from 0.820 in Daet to 0.931 in Manila. This implies that a small fraction of road nodes mediate a large share of shortest paths. The mechanism differs by urban type. Manila combines dense infrastructure with extreme flow concentration, suggesting potential vulnerability to corridor disruption. Smaller and rural cities show lower hierarchy but greater dependence on dispersed facilities and fewer redundant alternatives. Cross-source flood validation (presented below) indicates that agreement between NOAH and observational data varies systematically with urbanization, with weaker observational support in dense built environments.

Flood exposure. Project NOAH 5-year flood hazard polygons show distinct hazard regimes across the ten study cities (Fig. 3). Riverine cities such as Tuguegarao and Dagupan exhibit corridor-like hazard patterns that follow well-defined floodplains, consistent with prior flood mapping work (29). In contrast, highly urbanized areas such as Manila show more spatially dispersed hazard overlapping dense road networks.

Independent validation supports this distinction. Figure 2 presents four representative cities selected to illustrate variation in hazard pattern and validation strength. Satellite observations reproduce the same broad flood corridors in riverine cities such as Naga and Ilagan. In contrast, agreement is weaker in more urbanized settings, particularly in Manila and parts of San Fernando. These areas correspond to dense built environments in the GHSL layer, indicating that reduced agreement is associated with urban structure rather than a clear model failure.

This pattern is consistent with the full study sample (Fig. 9). City-level validation metrics show that agreement is stronger in cities where flood-prone areas occupy a larger share of the urban footprint, and weaker where hazard is concentrated in built-up terrain.

We use the 5-year return-period scenario because it represents a frequent, planning-relevant hazard rather than a rare catastrophic event. In the post-flood network experiment, road segments intersecting medium- or high-depth polygons are removed from the graph. Segments intersecting low-depth polygons are retained as passable.

The choice of a medium-depth cutoff is conservative with respect to field evidence from Metro Manila. Mamuyac et al. find that flood depths above 25 cm consistently caused lane closures and reduced vehicle flow by 40–70% per lane-kilometer as closures increased (28). Project NOAH categories are categorical rather than continuous, so the analysis treats the medium class (0.5–1.5 m) as the first reliably impassable category and retains the low class (0–0.5 m) for sensitivity testing.

Facility coverage and baseline access. OpenStreetMap facility coverage is uneven across service types. Schools are present in meaningful numbers in all cities, while hospitals and pharmacies are sparse in several cases. Ilagan has only two mapped hospitals and one mapped pharmacy, and Cotabato has ten hospitals and fourteen pharmacies. These counts reflect a mix of real service scarcity and incomplete tagging.

Baseline E2SFCA scores reveal a stable type hierarchy across all ten cities (Fig. 5). Schools score highest ($\sim 10^{-4}$

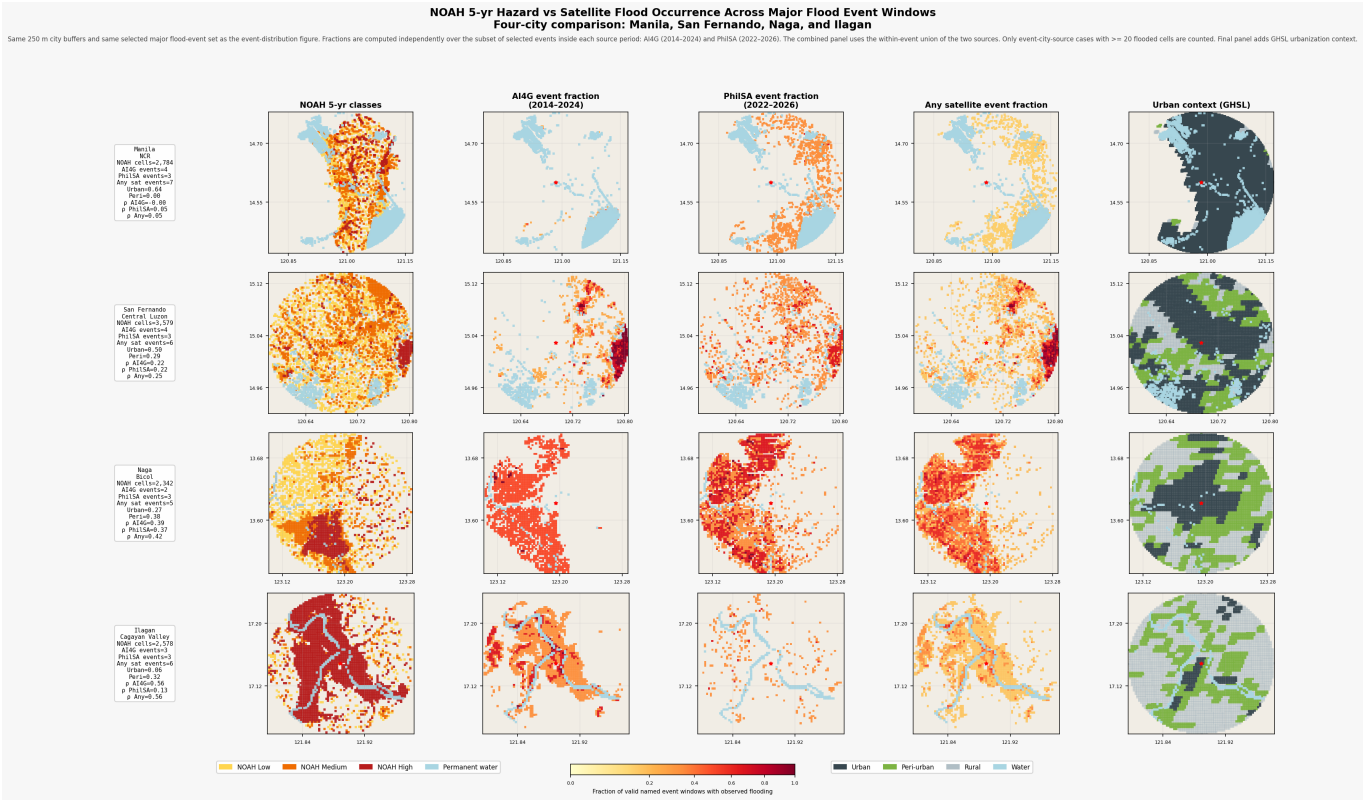

Fig. 2. Cross-source spatial support for Project NOAH hazard across four representative cities selected to illustrate variation in hazard pattern and validation strength. Columns show NOAH 5-year hazard classes, AI4G event fraction, PhilSA event fraction, the within-event union of the two satellite sources, and GHSL urban context.

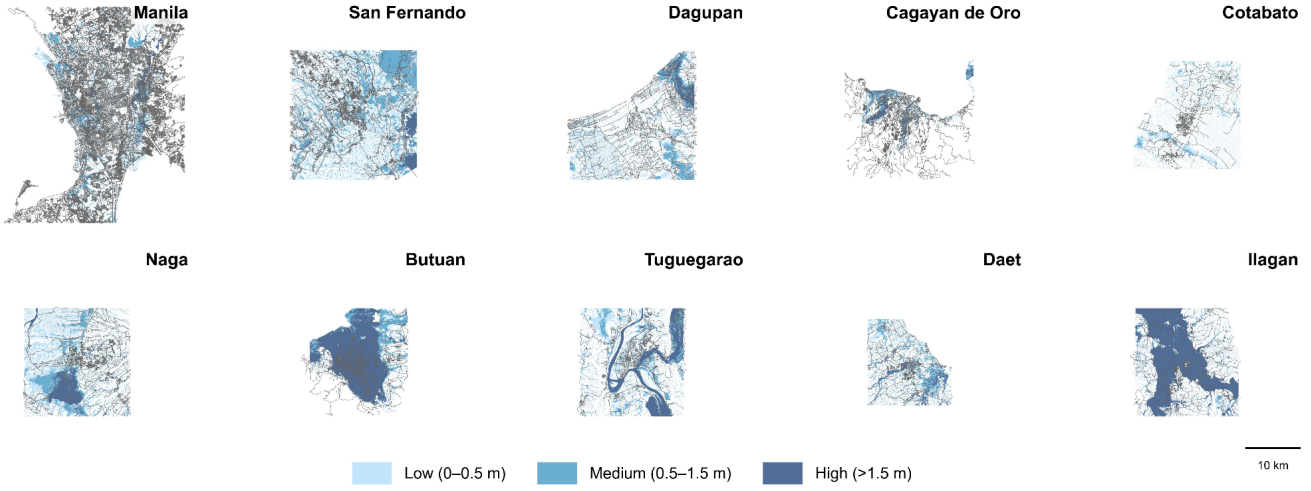

Fig. 3. Project NOAH 5-year flood hazard exposure by city. Light, medium, and dark blue represent low (0–0.5 m), medium (0.5–1.5 m), and high (>1.5 m) hazard classes. The edge-removal scenario treats medium and high polygons as disruptive to road travel.

to 10^{-3}), reflecting their abundance, while hospitals sit lowest ($\sim 10^{-5}$), consistent with fewer facilities spaced farther apart. Within-city inequality varies: Manila's hospital distribution is tight and unimodal, while Tuguegarao's spreads wide, with 1.5% of its population already scoring zero before any flooding. Markets show the widest gaps within cities, with some distributions splitting into well-served and underserved halves.

Crossing population density with market access reveals where the most people compete for the fewest facilities (Fig. 6). Red cells mark high population and low access. Peripheral Manila and core Cotabato are already underserved before any flood. These populations are more exposed to further access loss under disruption.

The spatial distribution of hospital access shows equity stakes (Supplementary Fig. S1). Dense cities such as Manila, Dagupan, and San Fernando maintain relatively high hospital accessibility across much of the urban extent, while several mid-size and smaller cities show core-periphery gradients. Tuguegarao and Ilagan have peripheral cells with very low or zero baseline hospital accessibility before any flood disruption is imposed.

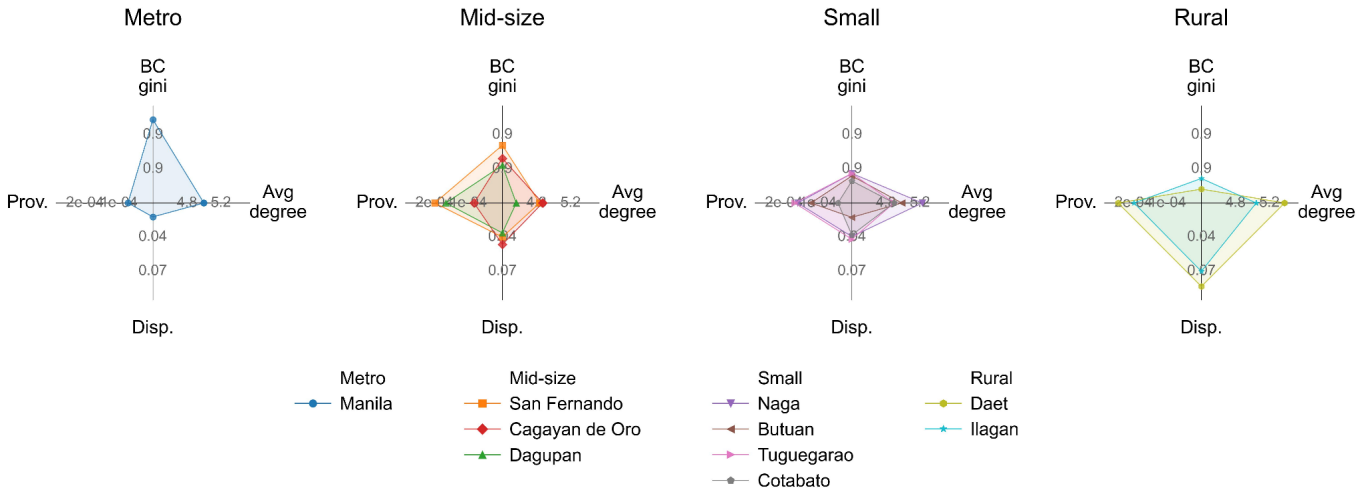

Fig. 4. Pre-flood structural vulnerability profiles by city group. Axes summarize betweenness-centrality concentration (BC Gini), average degree, facility provision, and facility dispersion. Manila's profile is dominated by high hierarchy, while smaller and rural cities tend to express vulnerability through facility dispersion and sparse service alternatives.

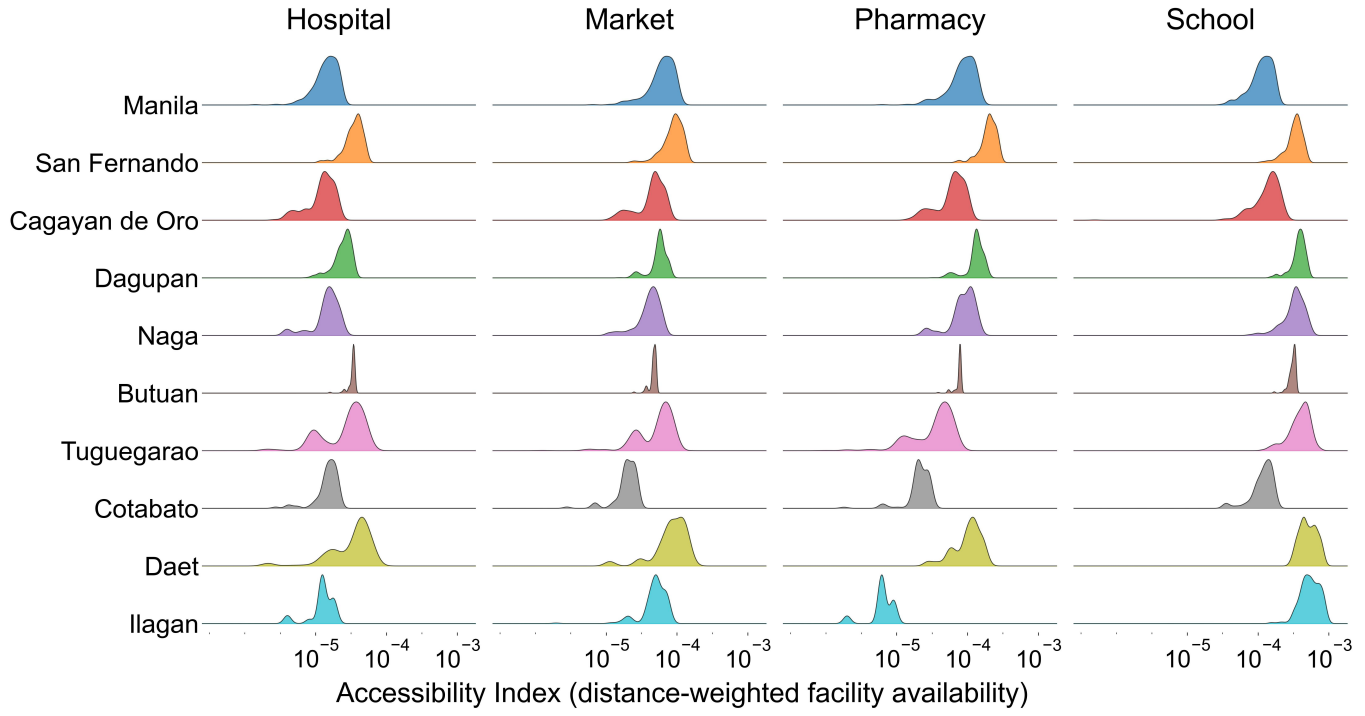

Fig. 5. Baseline accessibility distributions across ten cities and four facility types. Each ridge shows the density of E2SFCA scores across LandScan demand cells. Smaller cities have tighter spreads; markets show the widest within-city gaps. Schools are the most evenly distributed service type.

Flood disruption of service access. Removing road edges that intersect medium- or high-depth NOAH polygons produces sharply different outcomes depending on city structure (Table 2). The share of edges removed ranges from 1.4% in Cotabato, where flood polygons barely overlap the road network, to 74.0% in Butuan, where the Agusan River floodplain inundates most of the urban road system. Yet the relationship between edge loss and access loss is nonlinear. Naga loses 8.2% of edges but 18.9% of its population is affected, while Dagupan loses a comparable 7.8% of edges yet only 15.9% is affected. The difference reflects network topology: Dagupan's grid structure provides rerouting alternatives that Naga's more radial layout does not.

Three cities illustrate how road network structure differentiates flood impacts (Fig. 7). Dagupan loses 7% of road edges and 16% of the population is affected (market access), but its grid reroutes traffic around flooded segments, and 54% of affected residents are outside the flood zone. Tuguegarao loses 9% of edges and 26% of the population is affected; the Cagayan River bisects the network, and flooded bridges sever the east bank, producing an indirect share of 72%. Butuan loses 74% of edges, affecting 85% of the population in a near-total network collapse where most losses are direct (indirect share 13%). Flood maps miss the indirect population entirely.

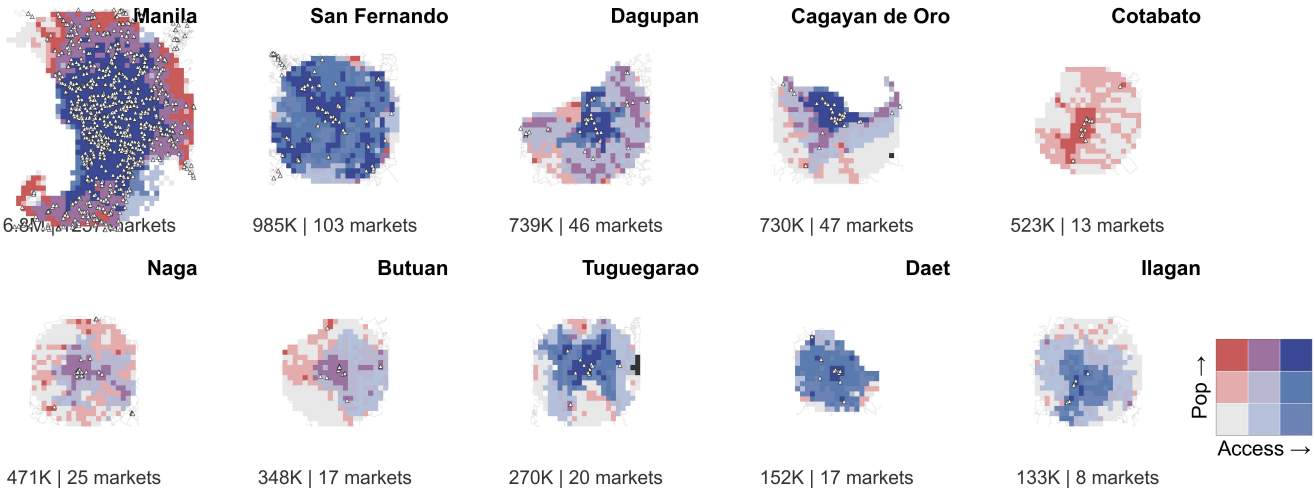

Fig. 6. Bivariate map of population density and market accessibility. Red cells have high population and low access; blue cells have low population and high access; purple cells have both. Triangles mark market locations. These pre-flood disparities identify which populations are exposed to further access loss.

Table 2. Flood disruption summary by city (market access).

City	Edges rm. (%)	Affected (%)	Indirect (%)
Butuan	74.0	84.7	13.1
Ilagan	40.1	97.3	42.3
Manila	10.9	19.4	51.4
Daet	10.2	21.9	77.2
San Fernando	10.1	27.1	61.5
Cagayan de Oro	9.5	25.2	70.7
Tuguegarao	9.5	25.6	71.9
Naga	8.2	18.9	46.9
Dagupan	7.8	15.9	53.6
Cotabato	1.4	1.9	64.9

Across all ten cities, the indirect share of market-access losses ranges from 13% (Butuan) to 77% (Daet) (Table 2). In seven of ten cities, more than half of affected residents are on dry land but lose access because flooded roads elsewhere sever their routes.

Disruption severity varies by service type but the network-mediation effect does not (Supplementary Table S2). Schools are the most resilient: 20% of population loses more than half of school access on average, compared to 32% for hospitals and 33% for pharmacies. This is consistent with the baseline finding that schools are more numerous and spatially dispersed, providing more rerouting alternatives. However, the indirect share is stable across types (55–59%), indicating that the proportion of access loss occurring outside flood zones is a structural property of the road network rather than a feature of any particular service geography.

Demographic profiles of accessibility disruption. We next examine whether modeled flood-related accessibility disruption is distributed evenly across populations. To do so, we aggregate LandScan-cell disruption measures to barangays using allocated LandScan population weights, then compare barangay demographic composition across city-specific quintiles of the total disruption proxy. Defining quintiles within city prevents the comparison from being driven only by differences between Manila and smaller cities.

The results show that disruption is not only an infrastructural outcome. Barangays in higher-disruption quintiles differ from lower-disruption barangays across several demographic dimensions, including sex composition, age structure, education, literacy, and functional difficulty (Fig. 8). These patterns suggest that flood-related road disruption can have different human implications depending on where socially or service-dependent populations are located.

These results are descriptive rather than causal. The analysis does not show that demographic composition causes disruption, nor that flooding changes demographic outcomes. Instead, it identifies which populations are located in barangays where modeled disruption to essential-service access is highest.

Cross-source flood validation. We compare Project NOAH 5-year hazard maps with independent observational flood products to assess whether NOAH is a defensible hazard layer for the downstream accessibility analysis. Project NOAH was developed as an operational hazards program for disaster prevention and mitigation in the Philippines (12), and the 5-year hazard layer used here comes from the Project NOAH archive (13).

The NOAH layer is a static hazard product. The observational layers are event-based detections from different sensors and time periods. We therefore do not expect exact spatial agreement. Instead, we evaluate whether observed flooding occurs in areas identified by NOAH, whether broad spatial patterns align across sources, and where support is stronger or weaker.

Across the four-city comparison (Fig. 2), NOAH receives strong independent support in riverine settings such as Naga and Ilagan, where satellite observations reproduce the same flood-prone corridors. In contrast, agreement is weaker in more urbanized areas, particularly in Manila and parts of San Fernando. These locations correspond to dense built environments in the GHSL layer, indicating that reduced agreement is associated with urban structure rather than a clear model failure.

At the city level, support metrics show the same pattern (Fig. 9). Across the ten cities, the share of

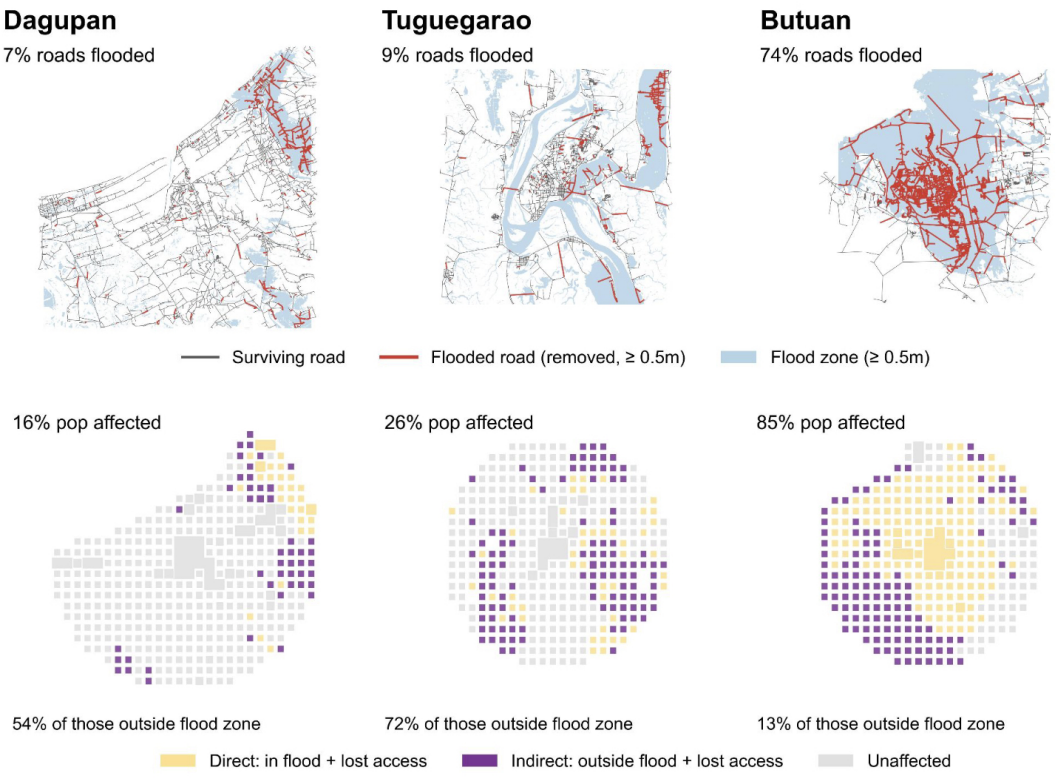

Fig. 7. Flood disruption in three case cities. Top row: road networks with surviving (gray) and removed (red) edges under the Var ≥ 2 threshold, over NOAH flood polygons (blue). Bottom row: market-access impact classified as direct (yellow: in flood zone and lost access), indirect (purple: outside flood zone but lost access through network-mediated route severance), or unaffected (gray). Dagupan's grid reroutes around damage; Tuguegarao's river crossing is a single point of failure; Butuan's floodplain removes most of the network.

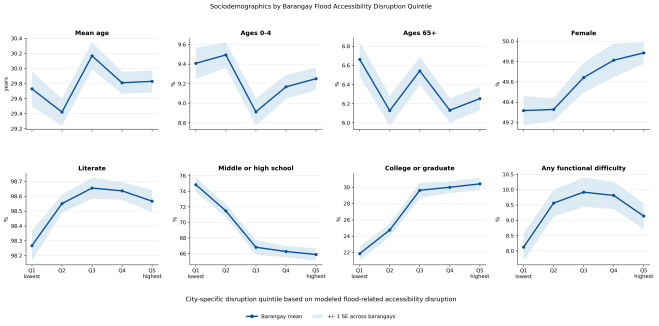

Fig. 8. Demographic composition across city-specific quintiles of flood-related accessibility disruption. Points show barangay means by disruption quintile; shaded bands show ± one standard error across barangays. Quintiles are computed within city so that the comparison captures relative disruption exposure inside each urban area rather than only differences across cities.

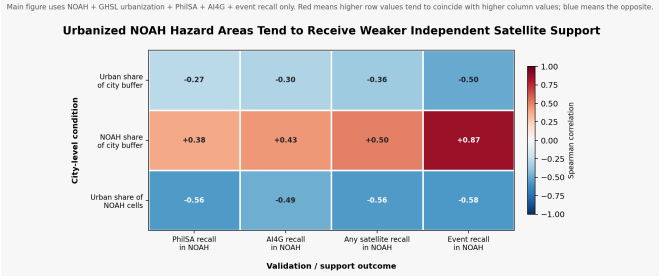

Fig. 9. City-level Spearman correlations linking NOAH support outcomes to urbanization and hazard pattern across the ten-city sample. Positive values indicate that higher values of a variable are associated with stronger observational support, while negative values indicate weaker support.

NOAH cells is positively associated with PhilSA recall in NOAH, AI4G recall in NOAH, and any-satellite recall in NOAH, with Spearman correlations of 0.38, 0.43, and 0.50, respectively. The strongest positive association is with event recall in NOAH ($\rho = 0.87$). By contrast, the urban share of NOAH cells is consistently negatively associated with these support measures ($\rho = -0.56, -0.49, -0.56$, and -0.58), indicating systematically weaker agreement in dense built environments, consistent with known limitations of satellite flood detection in urban areas (30, 31).

Groundsource is evaluated as an auxiliary observational reference but is not used as a primary validator. It shows high recall but low precision (see SI Table S3), indicating that it broadly overlaps hazard zones without precisely localizing flood extent. This makes it useful for confirming that flooding occurred near hazard areas, but not for detailed spatial validation.

Discussion

The baseline results suggest that flood vulnerability is not reducible to flood exposure alone. Network form, service distribution, and population geography jointly shape who can reach essential services before and after flooding. Manila's risk is partly a problem of hierarchy: the road network is dense, but shortest-path flow is strongly concentrated. Smaller cities express a different vulnerability: lower facility counts, wider facility dispersion, and more peripheral demand cells near the edge of the 30-minute catchment.

Table 3. Core modeling parameters.

Parameter	Value
Travel-time threshold	30 min
Decay weights	1.00 / 0.68 / 0.22
Sub-zone boundaries	10 / 20 / 30 min
Facility capacity	1 per facility
Flood removal threshold	NOAH Var ≥ 2
Dispersion reference speed	30 km/h
BC sample size	min(300, $\lvert V\rvert$)
Network representation	Undirected
Demand unit	LandScan cell

The NOAH Var ≥ 2 threshold corresponds to the medium and high categorical hazard classes. Low-depth polygons are retained as passable. Sensitivity tests at 15- and 20-minute thresholds confirm rank-order stability (Supplementary Table 1).

This distinction matters for policy. If flood planning only maps inundated places, it can miss households outside flood polygons that become isolated because connecting roads fail. A network-accessibility view instead identifies road segments whose protection would preserve service access for many residents, including residents who are not directly inundated. These segments are strong candidates for drainage improvements, elevation, emergency-routing protection, or targeted maintenance before recurring seasonal floods.

Sensitivity tests on two cities (Daet and Cotabato) confirm that cell-level accessibility rankings are stable across travel-time thresholds (Table S**??**). At 20 minutes, Spearman rank correlations against the 30-minute baseline exceed 0.87 for all service types. At 15 minutes, hospitals remain highly stable ($\rho > 0.95$) because they are sparse and catchment membership changes little, while schools are more sensitive ($\rho = 0.48$–0.78) because shorter thresholds exclude peripheral facilities. These results support the 30-minute default and are consistent with prior findings on rank-order stability across E2SFCA configurations (8).

A remaining limitation is that the demographic analysis should be interpreted as an exposure profile rather than a realized behavioral response. The model identifies barangays where residents are more exposed to service-access disruption under the road-removal scenario, but it does not observe actual post-flood trips, route choices, or substitutions across facilities. Future work should combine these modeled exposure profiles with observed mobility, facility-capacity data, and local emergency-routing information to distinguish potential accessibility loss from realized disruption.

Finally, while the model evaluates barangay-level vulnerability, further work must be done to be able to recommend specific infrastructure mitigations.

Materials and Methods

Study sample and data sources. The analysis uses ten Philippine cities selected from provinces highlighted in the WorldRiskReport 2025 local flood-exposure analysis. City radii range from 8 to 20 km and are centered on each city. Road networks and points of interest are extracted from OpenStreetMap using OSMnx (9, 10). Population demand comes from LandScan Global 2023, an ambient population raster at approximately 1-km resolution (11). Flood hazard comes from Project NOAH 5-year return-period flood polygons (12, 13). Flood validation uses multiple independent observational datasets. These include AI4G Sentinel-1 flood detections (29, 32), PhilSA satellite-derived flood extents (33), and Google Groundsource event data (34). These sources are used only for validation and are not applied in the road-removal model. Validation metrics are computed on a common grid by comparing NOAH hazard classifications with independent observational flood detections. Support is defined as the share of NOAH hazard cells with at least one observational hit from a given source, with an additional any-satellite metric defined as the union of AI4G and PhilSA detections. Urban context is derived from the GHSL GHS-SMOD R2023A settlement dataset (35), which classifies land into rural, peri-urban, and urban categories using the Degree of Urbanisation framework (36). PSA 2020 Census Data is finally used to look at potental demographic trends (14).

Road networks and facilities. Drivable OSM networks are downloaded by city center and radius. OSMnx imputes free-flow speed from `maxspeed` tags and highway-type defaults, then computes travel time for each edge as $\tau_e = \ell_e / v_e$. Directed graphs are converted to undirected graphs for E2SFCA routing because catchment membership assumes symmetric travel time. Essential-service facilities are extracted for four categories: hospitals (`amenity=hospital`), schools (`amenity=school`), markets (`shop=supermarket` or `amenity=marketplace`), and pharmacies (`amenity=pharmacy`). Polygon features are represented by centroids. Each facility is snapped to the nearest graph node with a KD-tree.

Population demand. LandScan cells are clipped to each city radius, and zero-population cells are dropped. Each remaining cell centroid is snapped to its nearest graph node with the same KD-tree procedure used for facilities. Population is retained at the cell level rather than aggregated to proxy nodes. Multiple cells may share a proxy node, but each cell retains its own population weight.

Enhanced two-step floating catchment area. For each facility j, the weighted population competing for it within the travel-time threshold d_0 is

$$D_j = \sum_{i:\tau_{ij} \leq d_0} W(\tau_{ij}) P_i,$$

where P_i is the population of demand cell i, τ_{ij} is network travel time from cell i to facility j, and $W(\cdot)$ is a step-wise distance-decay function. With equal facility capacity $S_j = 1$, the supply-to-demand ratio is $R_j = 1/D_j$. Cell-level accessibility is then

$$A_i = \sum_{j:\tau_{ij} \leq d_0} W(\tau_{ij}) R_j.$$

The catchment threshold is 30 min, divided into 0–10, 10–20, and 20–30 min sub-zones with weights 1.00, 0.68, and 0.22 following the slow-decay E2SFCA scheme (7). Under equal capacity, the population-weighted mean accessibility for a city-service pair equals the service's per-capita provision, which is used as a computational check.

Network structural metrics. Average degree is computed as $\bar{k} = 2|E|/|V|$ on the undirected graph. Betweenness centrality is approximated with $k = \min(300, |V|)$ sampled source nodes and seed 42. The betweenness Gini coefficient is computed from sorted betweenness values $b_1 \leq \cdots \leq b_n$ as

$$G_{BC} = \frac{2\sum_{i=1}^{n} i b_i}{n \sum_{i=1}^{n} b_i} - \frac{n+1}{n}.$$

Facility provision is the raw count of facilities per capita. Facility dispersion is the median nearest-neighbor network travel time among same-type facilities, normalized by the travel time implied by the city radius and a 30 km/h reference speed.

Flood disruption analysis. Road edges are spatially joined to NOAH flood polygons. In the main scenario, an edge is removed when its maximum overlapping hazard class satisfies Var ≥ 2, corresponding to medium or high modeled depth. E2SFCA is rerun on the degraded graph to produce A_i^{post}. The relative cell-level change is

$$\delta_i = \frac{A_i^{\text{post}} - A_i^{\text{base}}}{A_i^{\text{base}}}.$$

A cell is classified as affected if $\delta_i < 0$, i.e., any loss of accessibility. Affected cells are further classified as direct if the cell lies within a flood polygon and indirect if the cell lies outside all flood polygons but loses access because network routes are severed elsewhere. The indirect ratio is the affected outside-flood-zone population divided by total affected

population. City-level summaries also report the population share with severe access loss ($\delta_i < -0.5$) and the share newly disconnected ($A_i^{\text{base}} > 0$ and $A_i^{\text{post}} = 0$).

Reddit NLP and discourse map. In considering questions on the behavioral aspects of a population, and to validate the predictions and assumptions made in our physical models, we explored using natural language processing (NLP)-styled methods to give us preliminary insight into people's behavior during flood conditions, and confirmation for how they are affected by such conditions. This direction is informed by recent methodological literature by Hameed et al.(37) which uses LLMs to assist in geotagging disaster impact related Twitter/X posts to their corresponding locations on a map. Our result in this effort led to the creation of a geotagged map of Reddit threads which both discuss impacts of flooding and named locations.

To do this, we took some of the Subreddits most frequently used by people in the Philippines, picked a series of timeframes corresponding to either flood events or baseline, embedded the content, and used augmented retrieval to verify that we could recover conversations related to impacts on people's mobility and access to infrastructure, confirming that such discourse is taking place on Reddit. We then ran a series of data cleaning techniques to filter out bot and irrelevant data, string match against a geographical index, and enact a final LLM filter to parse for relevant threads that discuss both flood impacts and named geographical locations (Fig. S3).

Some known scope and limitations to the data: in 2025, internet usage penetration in the Philippines was estimated to be around 83.8 percent of the population, representing 98 million individuals (38). Of the internet-use population, 15.4 percent is estimated to have used Reddit based on advertisement statistics. While specific demographic information on Reddit users in the Philippines is not readily found, we use information on usage in the US to infer that, in general, Reddit users are typically male and at or below middle age (39). Moreover, our final geotagged map is limited to 35 threads from a start of 60,949 after the data cleaning and relevance filters were applied. These limitations, combined with the generally new methodology, lead us to decide that this approach is not yet ready as a validation for our physical models. In future work, we might look towards using more demographically representative, and frequented, social media data, such as Facebook.

Demographic linkage and barangay aggregation. To connect modeled accessibility disruption to population vulnerability, we link LandScan demand cells, barangay boundaries, and 2020 Philippine census demographic summaries. Because LandScan cells are coarser than many urban barangays, we allocate each cell to barangays by area overlap rather than assigning the full cell to a single polygon. We then allocate LandScan population proportional to the cell-area overlap. For each service type or total disruption proxy k, barangay-level disruption is computed as the allocated-population-weighted mean

$$Q_{bk} = \frac{\sum_{c \in b} \widetilde{P}_{cb} q_{ck}}{\sum_{c \in b} \widetilde{P}_{cb}},$$

where $\widetilde{P}_{cb}$ is allocated populaton and q_{ck} is the disruption proxy assigned to cell c and barangay b. We then divide barangays into city-specific quintiles of the total disruption proxy and compare demographic means across quintiles. This within-city ranking compares relatively high- and low-disruption barangays inside the same urban area, rather than allowing cross-city scale differences to dominate the comparison.

Implementation. Because the routing graph is undirected, both E2SFCA passes are computed from demand-node Dijkstra queries. Dijkstra searches use a sparse adjacency matrix with a 1,800-second cutoff. Demand cells sharing a proxy node are deduplicated during routing and then expanded back to cell-level scores. Cities are parallelized across workers. The Reddit corpus provides behavioral evidence of mobility disruption. Census demographic summaries are linked to barangays across all ten cities via area-weighted LandScan allocation.

Data, Materials, and Software Availability. All primary input datasets are publicly available from OpenStreetMap, LandScan Global 2023, Project NOAH or LiPAD hazard-map repositories, Google Groundsource, and Philippine census or administrative-boundary data sources subject to each provider's access terms. Analysis code and derived data are available at https://github.com/andersvestrum/flooding-infrastructure-Philippines.

ACKNOWLEDGMENTS. We thank Professor Joshua Blumenstock for feedback and the students of INFO 288 for comments and encouragement. We also thank members of the University of the Philippines Resilience Institute and Project NOAH community for the scientific data infrastructure that makes this analysis possible.

1. Buendnis Entwicklung Hilft and Institute for International Law of Peace and Armed Conflict. WorldRiskReport 2025: Focus: Floods. Technical report, Buendnis Entwicklung Hilft, Berlin, 2025. URL https://weltrisikobericht.de/worldriskreport/.
2. Philippine Atmospheric, Geophysical and Astronomical Services Administration. Tropical cyclone information, 2026. URL https://www.pagasa.dost.gov.ph/climate/tropical-cyclone-information. Accessed 2026-04-07.
3. Joseph Basconcillo and Noel Bangquiao. Recent increase in the number of Super Typhoons in the Philippines. *Tropical Cyclone Research and Review*, 2025. . URL https://doi.org/10.1016/j.tcrr.2025.09.001.
4. Weiping Wang, Saini Yang, H. Eugene Stanley, and Jianxi Gao. Local floods induce large-scale abrupt failures of road networks. *Nature Communications*, 10:2114, 2019. . URL https://doi.org/10.1038/s41467-019-10063-w.
5. Geoff Boeing and Jinwon Ha. Resilient by design: Simulating street network disruptions across every urban area in the world. *Transportation Research Part A: Policy and Practice*, 182:104016, 2024. . URL https://doi.org/10.1016/j.tra.2024.104016.
6. Ylenia Casali and Hans R. Heinimann. A topological characterization of flooding impacts on the Zurich road network. *PLOS ONE*, 14(7):e0220338, 2019. . URL https://doi.org/10.1371/journal.pone.0220338.
7. Wei Luo and Yi Qi. An enhanced two-step floating catchment area (E2SFCA) method for measuring spatial accessibility to primary care physicians. *Health & Place*, 15(4):1100–1107, 2009. . URL https://doi.org/10.1016/j.healthplace.2009.06.002.
8. Xiang Chen and Pengfei Jia. A comparative analysis of accessibility measures by the two-step floating catchment area (2SFCA) method. *International Journal of Geographical Information Science*, 33(9):1739–1758, 2019. . URL https://doi.org/10.1080/13658816.2019.1591415.
9. Geoff Boeing. OSMnx: New methods for acquiring, constructing, analyzing, and visualizing complex street networks. *Computers, Environment and Urban Systems*, 65:126–139, 2017. . URL https://doi.org/10.1016/j.compenvurbsys.2017.05.004.
10. OpenStreetMap contributors. OpenStreetMap, 2026. URL https://www.openstreetmap.org. Accessed 2026-04-07.
11. Oak Ridge National Laboratory. LandScan Global 2023, 2024. URL https://landscan.ornl.gov/. Accessed 2026-04-07.
12. Alfredo Mahar Francisco A. Lagmay, Bernadine Angelica Racoma, Kathryn Angelica Aracan, Julie Alconis-Ayco, and Ilene Saddi. Disseminating near-real-time hazards information and flood maps in the Philippines through Web-GIS. *Journal of Environmental Sciences*, 59:13–23, 2017. . URL https://doi.org/10.1016/j.jes.2017.03.014.
13. University of the Philippines NOAH Center. Project NOAH hazard maps, 2026. URL https://noah.up.edu.ph/. Accessed 2026-04-07.
14. Philippine Statistics Authority. Census of Population and Housing 2020: CPH Form 2 – Common Household Questionnaire Data Dictionary. Philippine Statistics Authority Data Archive, 2020. URL https://psada.psa.gov.ph/catalog/231/data-dictionary/F5?file_name=CPH%20Form%202%20-%20Common%20Household%20Questionnaire. Reference ID: PHL-PSA-CPH-2020-v1.0. Created May 8, 2023; last modified May 15, 2024. Accessed May 4, 2026.
15. Geoff Boeing. Osmnx: New methods for acquiring, constructing, analyzing, and visualizing complex street networks. *Computers, Environment and Urban Systems*, 65:126–139, 2017. .
16. Geoff Boeing and Yiming Zhou. Travel time prediction from sparse open data. *International Journal of Geographical Information Science*, 2026. . Published online ahead of print.
17. Wei Luo and Yi Qi. An enhanced two-step floating catchment area (E2SFCA) method for measuring spatial accessibility to primary care physicians. *Health & Place*, 15(4):1100–1107, 2009. .
18. Xiang Chen and Pengfei Jia. A comparative analysis of accessibility measures by the two-step floating catchment area (2SFCA) method. *International Journal of Geographical Information Science*, 33(9):1739–1758, 2019. .
19. Weiping Wang, Saini Yang, H. Eugene Stanley, and Jianxi Gao. Local floods induce large-scale abrupt failures of road networks. *Nature Communications*, 10:2114, 2019. .
20. Chao Fan, Xuan Jiang, and Ali Mostafavi. A network percolation-based contagion model of flood propagation and recession in urban road networks. *Scientific Reports*, 10:13481, 2020. .
21. Geoff Boeing and Jinwon Ha. Resilient by design: Simulating street network disruptions across every urban area in the world. *Transportation Research Part A: Policy and Practice*, 182:104016, 2024. .
22. Ylenia Casali and Hans R. Heinimann. A topological characterization of flooding impacts on the Zurich road network. *PLOS ONE*, 14(7):e0220338, 2019. .
23. Sofia Loreti, Enrico Ser-Giacomi, Andreas Zischg, Margreth Keiler, and Marc Barthelemy. Local impacts on road networks and access to critical locations during extreme floods. *Scientific Reports*, 12:1552, 2022. .
24. Utkarsh Gangwal and Shimao Dong. Critical facility accessibility rapid failure early-warning detection and redundancy mapping in urban flooding. *Reliability Engineering & System Safety*, 224:108555, 2022. .
25. Ali Esmalian, Nicole Coleman, Fang Yuan, Xue Xiao, and Ali Mostafavi. Characterizing equitable access to grocery stores during disasters using location-based data. *Scientific Reports*, 12:20203, 2022. .
26. Kristen Best, Qian He, Allison C. Reilly, Deb A. Niemeier, Michael Anderson, and Tom Logan. Demographics and risk of isolation due to sea level rise in the United States. *Nature Communications*, 14(1):7904, 2023. .

27. Josiah L. Kephart, Usama Bilal, Nelson Gouveia, Olga L. Sarmiento, Emily Shingara, Karina Rangel Moreno, Maryia Bakhtsiyarava, Juan Pablo Rodriguez, Sandra Ayala, Gabriel Carrasco-Escobar, and Ana V. Diez Roux. Social disparities in neighborhood flood exposure in 44,698 urban neighborhoods in Latin America. *Nature Cities*, 2:246–253, 2025. .
28. Lance Kenneth D. Mamuyac, Jon Robin D. Delos Reyes, Louisse Shaola L. Lumanglas, Eian Lanz C. Rebotiaco, Atsushi Fukuda, and Alexis M. Fillone. Flood-induced effects on vehicular traffic in Metro Manila, Philippines. *Natural Hazards*, 121(12):14907–14933, 2025. . URL https://doi.org/10.1007/s11069-025-07382-1.
29. Amit Misra, Kevin White, Simone Fobi Nsutezo, William Straka III, and Juan Lavista. Mapping global floods with 10 years of satellite radar data. *Nature Communications*, 16:5762, 2025. . URL https://doi.org/10.1038/s41467-025-60973-1.
30. Laura Giustarini, Renaud Hostache, Patrick Matgen, Guy J.-P. Schumann, Paul D. Bates, and David C. Mason. A change detection approach to flood mapping in urban areas using terrasar-x. *IEEE Transactions on Geoscience and Remote Sensing*, 51(4):2417–2430, 2013. . URL https://doi.org/10.1109/TGRS.2012.2210901.
31. Yu Li, Sandro Martinis, Marc Wieland, Stefan Schlaffer, and Ryo Natsuaki. Urban flood mapping using sar intensity and interferometric coherence via bayesian network fusion. *Remote Sensing*, 11(19):2231, 2019. . URL https://doi.org/10.3390/rs11192231.
32. Amit Misra. ai4g-flood-dataset, 2025. URL https://huggingface.co/datasets/ai-for-good-lab/ai4g-flood-dataset. Hugging Face dataset; accessed 2026-05-03.
33. Philippine Space Agency. PhilSA flood extent datasets for the philippines. Humanitarian Data Exchange (HDX), 2026. URL https://data.humdata.org/organization/philsa. Collection of event-specific satellite-derived flood extent shapefiles used in this study; accessed 2026-04-14.
34. Oleg Zlydenko, Rotem Mayo, and Deborah Cohen. Introducing Groundsource: Turning news reports into data with Gemini. Google Research Blog, 2026. URL https://research.google/blog/introducing-groundsource-turning-news-reports-into-data-with-gemini/. Accessed 2026-04-07.
35. Marcello Schiavina, Michele Melchiorri, and Martino Pesaresi. GHS-SMOD R2023A – GHS settlement layers, application of the degree of urbanisation methodology (stage i) to GHS-POP R2023A and GHS-BUILT-S R2023A, multitemporal (1975–2030). European Commission, Joint Research Centre [Dataset], 2026. URL https://data.jrc.ec.europa.eu/dataset/a0df7a6f-49de-46ea-9bde-563437a6e2ba.
36. European Commission and Statistical Office of the European Union. Applying the degree of urbanisation: A methodological manual to define cities, towns and rural areas for international comparisons. Technical report, Publications Office of the European Union, Luxembourg, 2021. URL https://doi.org/10.2785/706535.
37. Sameeah Noreen Hameed, Surangika Ranathunga, Raj Prasanna, Kristin Stock, and Christopher B. Jones. Extracting Disaster Impacts and Impact Related Locations in Social Media Posts Using Large Language Models, November 2025. URL http://arxiv.org/abs/2511.21753. arXiv:2511.21753 [cs] version: 1.
38. Simon Kemp. Digital 2026: The philippines. DataReportal, 2025. Retrieved May 3, 2026 from https://datareportal.com/reports/digital-2026-philippines.
39. Christopher St. Aubin and Jacob Liedke. Social media and news fact sheet. Pew Research Center, 2025. Retrieved May 3, 2026 from https://www.pewresearch.org/journalism/fact-sheet/social-media-and-news-fact-sheet/.